atmosphere

MDPI

*Article*

# Chemical Characterization and Source Apportionment of $PM_{2.5}$ During Autumn and Winter in an Industrial High-Tech Zone of the Yangtze River Delta, China

**Xiaochu He [1,2], Lei Jiang [1,*], Chenyu Yao [1], Jiahui Fan [1], Laihong Zhang [1], Yunpeng Liu [1] and Xinsheng Zhu [1,*]**

[1] Nanjing Institute of Environmental Sciences, Ministry of Ecology and Environment of the People's Republic of China, Nanjing 210042, China; hexc@saes.sh.cn (X.H.); yaochenyu@nies.org (C.Y.); fanjiahui@nies.org (J.F.); zhanglaihong@nies.org (L.Z.); liuyunpeng@nies.org (Y.L.)

[2] Shanghai Academy of Environmental Sciences, Shanghai 200233, China

* Correspondence: jianglei1836209@163.com (L.J.); zxs_dream@yeah.net (X.Z.)

**Abstract**

This study investigated the chemical composition and sources of $PM_{2.5}$ during autumn and winter in an industrial high-tech zone in the western Yangtze River Delta. Intensive sampling was conducted from November 2024 to January 2025. Nitrate ($NO_3^-$), sulfate ($SO_4^{2-}$), and ammonium ($NH_4^+$) were the predominant water-soluble ions, accounting for 62.8–91% of the total. The mean sulfur oxidation ratio (SOR = 0.365) and nitrogen oxidation ratio (NOR = 0.207) indicated significant secondary transformation. Principal component analysis of the eight water-soluble ions retained three components explaining 40.9%, 29.0% and 16.5% of the total variance (86.4% cumulatively), with loadings indicating a secondary inorganic salt/cooking mixture, a dust/industrial mixture and a cooking-related source. From clean to polluted periods, $NH_4^+$ and $NO_3^-$ concentrations increased significantly, indicating ammonium nitrate as a key driver of $PM_{2.5}$ accumulation. Positive matrix factorization resolved seven factors; after reallocating secondary aerosols to primary sources based on local emission inventories, industrial sources contributed the most (39.6%), followed by mobile sources (14.6%), fugitive dust (11.9%), cooking (11.9%), coal combustion (11.4%), and other sources (10.6%). These findings suggest that $PM_{2.5}$ mitigation in this zone should prioritize industrial-emission control, with coordinated reductions in NOx and $NH_3$ to curb ammonium nitrate-driven pollution.

**Keywords:** water-soluble ions; source apportionment; positive matrix factorization (PMF); industrial high-tech zones; Yangtze River Delta region

Check for updates

Academic Editor: Antonio Donateo

Received: 22 September 2026
Revised: 9 November 2026
Accepted: 10 November 2026
Published: 18 November 2026

**Copyright:** © 2026 by the authors. Licensee MDPI, Basel, Switzerland. This article is an open access article distributed under the terms and conditions of the Creative Commons Attribution (CC BY) license.

## 1. Introduction

Fine particulate matter ($PM_{2.5}$) remains a pressing environmental and public health concern in China, despite substantial reductions in ambient concentrations following the implementation of the Air Pollution Prevention and Control Action Plan and subsequent clean air policies. Recent studies have confirmed that the contribution of nitrate ($NO_3^-$) within secondary inorganic aerosols (SIAs) continues to rise, and it has replaced sulfate ($SO_4^{2-}$) as the main inorganic component of $PM_{2.5}$ in China [1–4]. This "nitrate-driven" pollution pattern is particularly prominent in densely populated regions including the Yangtze River Delta (YRD), the Beijing–Tianjin–Hebei region, and the Fenwei Plain [1]. Studies show that this shift is mainly caused by effective control of sulfur dioxide ($SO_2$) emissions, paired with relatively delayed mitigation of nitrogen oxides (NOx) and ammonia ($NH_3$) emissions [5,6]. Real-time monitoring conducted in northern cities such as

Xi'an, Shijiazhuang, and Beijing has found that during peak pollution periods, the mass fraction of nitrate in $PM_{2.5}$ can exceed 30%, and its formation rate is non-linearly regulated by atmospheric oxidation capacity (AOC) and relative humidity (RH). Furthermore, the contribution of secondary organic aerosols (SOAs) cannot be ignored. Winter observation conducted in typical cities like Shaoxing found that secondary organic carbon (SOC) accounted for as much as 47.3% of total organic carbon (OC), which indicates that the atmospheric oxidative transformation of volatile organic compounds ($VOC_S$) is a key driver of $PM_{2.5}$ mass growth [7]. In southwestern regions such as Chengdu and Chongqing, although the overall $PM_{2.5}$ concentration is lower than that in northern China, SIAs and total carbonaceous species (TC) still make up the main components of $PM_{2.5}$, showing clear seasonal fluctuation characteristics [8,9]. In the YRD region, a source apportionment study has reported that secondary inorganic aerosol sources contribute 35–50% of total $PM_{2.5}$ mass, followed by industrial sources, vehicle emissions, coal combustion, and dust [10]. A one-year observation carried out in suburban Nanjing further found that winter nitrate and SOAs share the same sources, and low temperature combined with high RH promotes their aqueous-phase formation [11]. A study covering six cities in Jiangxi Province also revealed city-specific source structures: secondary formation and combustion dominate pollution in Nanchang, industrial and vehicular emissions are the main sources in Jiujiang, and agricultural ammonium ($NH_4^+$) and traffic emissions are the main contributors in Pingxiang [12]. During heavy pollution events, the disproportionate growth of nitrate and ammonium, promoted by high atmospheric oxidation capacity, elevated RH, and abundant $NH_3$, has been identified as a key mechanism for winter haze formation in eastern China [13–16].

Compared with traditional urban monitoring sites, industrial parks and high-tech development zones have more complex emission spectra, covering centralized industrial combustion, production process emissions, heavy-duty diesel vehicle transportation, and fugitive dust. As a core tool for source apportionment, the positive matrix factorization (PMF) model can resolve these mixed sources more accurately by incorporating error weight matrices [17,18]. During a regional haze event in Nanjing, a comparison between principal component analysis (PCA) and the PMF model showed that PMF can separate the contributions of industrial emissions and secondary transformation more precisely, revealing how dominant sources dynamically evolve across different pollution stages [19]., A study on industrial clusters has confirmed that coal fly ash and soil dust are the dominant primary particulate forms in $PM_{2.5}$, while the PMF model quantifies the contribution of various primary emission sources to the total $PM_{2.5}$ mass. Notably, the role of $NH_3$ in $PM_{2.5}$ formation in industrial parks has become increasingly prominent. Four-season monitoring conducted in Xinxiang City showed that the seasonal fluctuation of water-soluble inorganic ions is highly consistent with that of $PM_{2.5}$: a sufficient supply of $NH_4^+$ promotes the neutralization of sulfates and nitrates, which in turn increases the hygroscopic growth and light scattering efficiency of particulate matter [20]. A study conducted by Guo et al. in typical industrial areas of northwest China found that water-soluble inorganic ions are the primary component of $PM_{2.5}$, with sulfate, nitrate and ammonium (SNA) accounting for more than 60% of the total mass, and the contribution of $SO_4^{2-}$ to $PM_{2.5}$ increases as pollution worsens [21]. A source apportionment study covering two districts of Lanzhou found that $NO_3^-$ accounts for 52.3% of secondary aerosols and that this is closely associated with atmospheric gas precursors [22]. Furthermore, combining machine learning methods such as Random Forest with PMF have further revealed the non-linear driving effects of meteorological parameters and precursor gases on the sulfur oxidation ratio (SOR) and nitrogen oxidation ratio (NOR) [23]. These findings highlight the necessity of conducting zone-specific source apportionment research to support the development of targeted control strategies for industrial high-tech zones.

In summary, $PM_{2.5}$ pollution in China has entered a new stage dominated by nitrate and secondary organic aerosols, and industrial parks have become a key focus and major difficulty in pollution governance due to their unique emission structures. In this study, we conducted a comprehensive chemical characterization and source apportionment of $PM_{2.5}$ during the autumn and winter seasons in the CH High-Tech Zone (due to certain corporate data management requirements, we are unable to provide the specific name and address of this zone; we use CH to replace the actual name of the industrial zone), an industrial development zone located in the western YRD region. The specific objectives are: (1) to characterize the $PM_{2.5}$ mass concentration and chemical composition, including water-soluble ions, carbonaceous fractions, and inorganic elements, based on an intensive field sampling campaign; (2) to investigate the role of water-soluble ions in $PM_{2.5}$ pollution, covering their concentration levels, source identification via principal PCA, acid–base balance, secondary transformation ratios (SOR and NOR), and evolution across different $PM_{2.5}$ pollution levels; and (3) to apportion $PM_{2.5}$ sources using the EPA PMF 5.0 receptor model, combined with SOA estimation via the EC-tracer method and reapportionment of secondary sources based on local emission inventories. The findings are expected to provide a scientific basis for formulating zone-specific $PM_{2.5}$ control strategies for industrial high-tech zones and contribute to a broader understanding of the chemical composition and source apportionment of wintertime $PM_{2.5}$ in the YRD region.

## 2. Materials and Methods

### *2.1. Study Area*

This study was conducted in a high-tech zone along the Yangtze River in the western YRD region. The region has a subtropical monsoon climate with four distinct seasons. The annual average temperature is 15.7 °C, the annual average precipitation is 1004.2 mm, and the annual average wind speed is 3.3 m/s. The dominant wind direction is northeast, with a calm wind frequency of 25.6%. The CH High-Tech Zone is a major industrial cluster hosting 64 gas-emitting enterprises within a 5 km radius of the national monitoring station. The industries include ferrous metal casting, machinery manufacturing, coatings, electronics, iron smelting, food processing, and advanced materials. Key enterprises include a coal-fired power plant, cement production, chemical and titanium dioxide manufacturing, foundry operations, and pharmaceutical enterprises.

### *2.2. $PM_{2.5}$ Sample Collection*

Intensive ambient $PM_{2.5}$ sampling was conducted during autumn and winter, from 25 November 2024 to 13 January 2025. A total of 50 daily $PM_{2.5}$ samples were collected. Two intelligent medium-flow samplers were deployed side by side at the monitoring site, where each unit was microcomputer-controlled and maintained constant flow by comparing the measured Venturi-tube flow with the set point and adjusting the pump speed. The PM2.5 size selection was provided by a size-selective impactor cut head mounted on the inlet (cut-off diameter D = 2.5 ± 0.2 μm; geometric standard deviation $\sigma g$ = 1.2 ± 0.1); before each sampling period, the cut head was disassembled, washed, dried, resealed and checked for leaks. Polypropylene fiber filter membranes were used for the analysis of inorganic elements and water-soluble ions, while quartz fiber filter membranes were used for carbonaceous component (OC/EC) analysis. Prior to sampling, polypropylene filters were baked at 60 °C for 2 h, and quartz filters were pre-fired at 500 °C for 4 h to remove residual organic contaminants. All filters were equilibrated in a controlled environment (20 ± 1 °C, 40 ± 3% RH) for at least 24 h before and after sampling and weighed using a Mettler XS204 analytical balance. The meteorological data and gaseous pollutant concentrations were obtained from the national monitoring station.

Source samples were collected for PMF analysis, including road dust, industrial chemical dust, casting/smelting dust, construction dust, and coal smoke dust. Road dust samples were collected from two road sections with high traffic volume. Coal smoke dust samples were collected from the flue gas stack of a power plant within the High-Tech Zone. Construction dust samples were obtained from cement mill dust and from active construction sites. Casting/smelting dust samples were collected from the dust removal systems of three casting enterprises. Industrial chemical dust samples were collected from the cyclone dust collection ash of a daily chemical company and from fugitive dust emissions during manual packaging operations. All source samples were sieved through a nylon sieve and then sealed for chemical analysis. Details of the chemical analysis procedures can be found in Text S1.

### *2.3. Data Analysis Methods*

#### 2.3.1. Principal Component Analysis (PCA) and Sulfur/Nitrogen Oxidation Ratios

PCA was applied to the eight water-soluble ion concentration datasets to identify potential source categories. PCA is a multivariate statistical technique that transforms a set of correlated variables into a smaller number of uncorrelated principal components through orthogonal transformation, thereby reducing data dimensionality while retaining most of the variance. The Kaiser–Meyer–Olkin (KMO) measure and Bartlett's test of sphericity were used to assess data suitability. Factors with eigenvalues greater than 1 were retained, and varimax rotation was applied to enhance the interpretability of factor loadings. Factors were interpreted based on the chemical species with high factor loadings and the known source associations.

SOR and NOR were calculated to evaluate the degree of secondary transformation of gaseous $SO_2$ and $NO_2$ into particulate $SO_4^{2-}$ and $NO_3^-$, respectively; the calculation formulas are given as follows:

$$SOR = \frac{c\left(SO_4^{2-}\right)}{c\left(SO_4^{2-}\right) + c(SO_2)} \quad (1)$$

$$NOR = \frac{c(NO_3^-)}{c(NO_3^-) + c(NO_2)} \quad (2)$$

where $c\left(SO_4^{2-}\right)$, $c(NO_3^-)$ and $c(SO_2)$, $c(NO_2)$ represent the molar concentrations of $SO_4^{2-}$ and $NO_3^-$ in $PM_{2.5}$ and $SO_2$ and $NO_2$ in the atmosphere, respectively, with unit mol $m^{-3}$. SOR and NOR values greater than 0.1 indicate that secondary transformation is the dominant process for the formation of the corresponding particulate ions, with higher values indicating greater conversion efficiency.

#### 2.3.2. Positive Matrix Factorization (PMF) and Reapportionment of Secondary Sources

The EPA PMF 5.0 model was used for quantitative source apportionment of $PM_{2.5}$. PMF decomposes the receptor chemical composition matrix $X$ (n samples × m species) into two non-negative matrices: factor contribution $G$ (n × p) and factor profile F (p × m), plus a residual matrix E:

$$X = GF + E \quad (3)$$

The model minimizes the objective function Q, defined as the sum of squared residuals weighted by the measurement uncertainty (uij):

$$Q = \Sigma\,\Sigma\,(eij/uij)^2 \quad (4)$$

A total of 25 chemical species were selected as model inputs, including $PM_{2.5}$ mass, 8 water-soluble ions ($Na^+$, $NH_4^+$, $K^+$, $Ca^{2+}$, $Mg^{2+}$, $Cl^-$, $NO_3^-$, and $SO_4^{2-}$), POC, EC, and 14 inorganic elements (Al, Si, S, K, Cl, Ca, Ti, V, Ba, Mn, Fe, Ni, Cu, and Zn). In total, 34

chemical species (24 elements + 8 ions + OC and EC) plus PM2.5 mass were measured and screened, and species with low concentration or without source specificity (e.g., Cr and Pb) were not entered. Species were classified by signal-to-noise ratio (S/N) as "strong" (S/N > 1), "weak" (0.5 ≤ S/N < 1), or "bad" (S/N < 0.5), with only strong and weak species being retained. Exploratory runs were conducted with factor numbers ranging from 4 to 9. The optimal seven-factor solution was selected based on the minimum Q value closest to the sample-species product, good agreement between observed and predicted concentrations ($R^2 > 0.6$, slope near 1, and intercept near 0), residuals within ±3, bootstrap factor mapping > 80%, and physically interpretable source profiles. Uncertainty analysis was performed using bootstrap, displacement, and bootstrap–displacement methods, with Fpeak runs confirming solution stability (dQ < 5%).

The PMF-resolved secondary inorganic aerosols (SIAs) and the pre-estimated SOAs were reapportioned to primary source categories in a separate, model-independent, assumption-dependent bookkeeping step that is reported separately from the PMF solution. The PMF-resolved SIA factor (11.39% of $PM_{2.5}$) was distributed in proportion to sectoral $SO_2$+NOx emission shares (industrial 85.42%, road mobile 6.57%, and non-road mobile 8.01%), and the pre-estimated SOAs (18.43% of $PM_{2.5}$), in proportion to sectoral VOC emission shares (industrial 89.11%, road mobile 4.82%, non-road mobile 2.35%, storage and transport 2.80%, and cooking fumes 0.93%) (Table S1). The allocation keys were taken from the latest atmospheric emission source inventory provided by the local government, specifically the most recent inventory with consistent sectoral resolution covering the study area; for context, the emission totals reported for the zone are 637.33 t $SO_2$, 1360.88 t NOx, 1379.8 t particulate matter and 261 t VOCs, and 64 gas-emitting enterprises lie within 5 km of the monitoring station. Sector-resolved $NH_3$ emissions are not available in this inventory, so $NH_3$ could not be used as an allocation key. The field survey identified a dominant local industrial $NH_3$ source, whereas agricultural and livestock sources within the park boundary are limited, so the $NH_3$ enabling ammonium nitrate formation in the study area is itself largely industrial and is consistent with the industry-dominant $SO_2$+NOx allocation keys.

#### 2.3.3. EC-Tracer Estimation of Secondary Organic Aerosols

The primary and secondary organic carbon fractions were separated using the EC-tracer (minimum OC/EC) method: SOC = OC − EC × (OC/EC)min; POC = OC − SOC; SOA = 1.6 × SOC. Here, (OC/EC)min is the minimum of the daily OC/EC ratios after excluding anomalous samples identified from the measured OC and EC, together with the SOA share of 18.43% of $PM_{2.5}$, and OM/OC = 1.6 is a conversion factor for aged urban aerosols, yielding POC = 3.82, SOC = 7.53 and SOA = 12.04 μg/m$^3$. The method assumes that sources are sufficiently stable for EC and primary OC to be co-emitted, such that the minimum OC/EC ratio represents the primary ratio. Because POC scales linearly with (OC/EC)min, the SOA estimate is regarded as semi-quantitative. The resulting carbon fractions are reported in Table S2 in concentration units and in clearly defined percentages.

## 3. Results

### *3.1. Characteristics and Chemical Composition of $PM_{2.5}$ Mass Concentration*

During the autumn and winter sampling period, the manually measured $PM_{2.5}$ concentrations at the CH monitoring station ranged from 21.1 to 123 μg/m$^3$, with an average value of 65.32 ± 17.96 μg/m$^3$. Among the 50 sampling days, $PM_{2.5}$ concentrations exceeded the National Secondary Air Quality Standard (75 μg/m$^3$) on 12 days, and the highest concentration of 123 μg/m$^3$ was recorded on December 6, 2024, corresponding to moderate air pollution; the meteorological conditions during this period can be found in Text S2 and Figure S1.

As shown in Figure 1 and Table 1, chemical speciation of $PM_{2.5}$ during the campaign revealed that water-soluble ions dominated the particulate mass (45.71 μg/m$^3$, 70.0% of $PM_{2.5}$), followed by carbonaceous species (OC + EC, 17.45 μg/m$^3$, 26.7%) and inorganic elements (3.59 μg/m$^3$, 5.5%). The element sum excludes S and Cl (counted as sulfate and chloride in the ion category) and Na, K, Ca and Mg (counted as water-soluble cations), so that the categories are strictly non-overlapping and the resulting mass closure is 102.2%. Expressed as the means ± SDs of the daily mass fractions, the corresponding fractions are 60.4% ± 15.6% for ions, 26.2% ± 14.9% for the carbonaceous fraction and 12.2% ± 6.2% for the XRF element sum as measured. These day-weighted statistics differ from the mass-weighted ratios of the campaign-mean concentrations given above because $PM_{2.5}$ mass and composition covary from day to day. Inorganic element concentrations remained relatively stable, whereas water-soluble ions and carbonaceous fractions exhibited substantial fluctuations driven by meteorological conditions and precursor emissions. During pollution episodes, water-soluble ions displayed the most pronounced concentration increases, while carbonaceous species also rose moderately. This underscores the dominant role of secondary inorganic formation in driving $PM_{2.5}$ escalation [24,25].

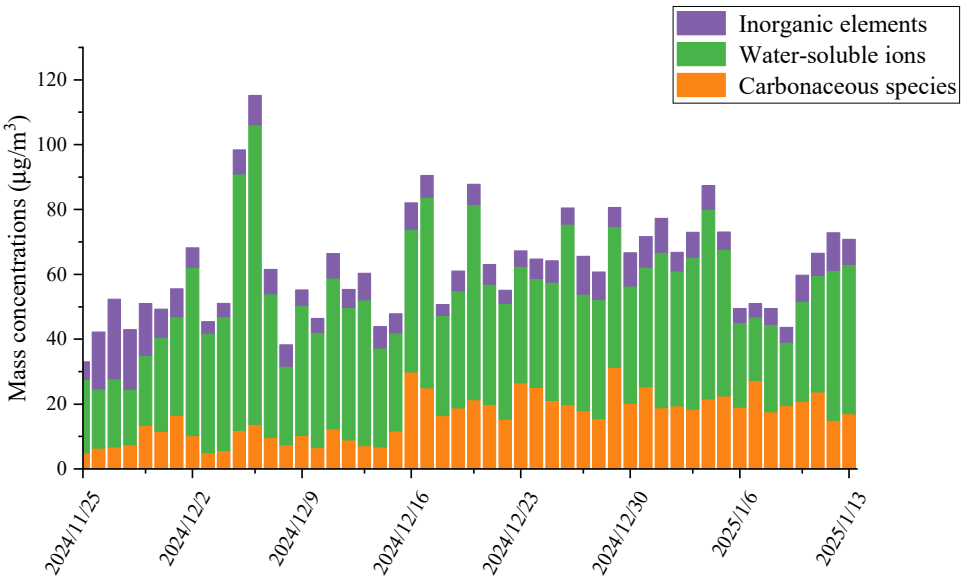



**Figure 1.** Temporal variation in $PM_{2.5}$ mass concentration and its major chemical component categories during the sampling campaign.

**Table 1.** Revised $PM_{2.5}$ mass closure and campaign-mean concentrations.

| Category | Species Included | Concentration (μg/m$^3$) | % of $PM_{2.5}$ |
|---|---|---|---|
| Water-soluble ions | $Cl^-$, $SO_4^{2-}$, $NO_3^-$, $Na^+$, $NH_4^+$, $K^+$, $Ca^{2+}$, and $Mg^{2+}$ | 45.71 | 70.0 |
| Carbonaceous species | OC + EC | 17.45 | 26.7 |
| Inorganic elements (XRF), excl. S, Cl, Na, K, Ca, and Mg | Al, Si, Ti, V, Cr, Ba, Sn, Mn, Fe, Co, Ni, Cu, Zn, etc. | 3.59 | 5.5 |
| Mass closure | | 66.75 | 102.2 |
| Memo: Inorganic elements (XRF), excl. S and Cl | | 69.54 | 106.5 |
| Memo: Inorganic elements | | 71.76 | 109.9 |

Among inorganic elements, Ca exhibited the highest mean concentration (1.701 ± 1.240 μg/m$^3$), followed by Cl (1.174 ± 0.581 μg/m$^3$), Si (1.065 ± 1.246 μg/m$^3$), Fe (0.624 ± 0.586 μg/m$^3$), and K (0.691 ± 0.278 μg/m$^3$). Ca and Si are typical crustal

elements, primarily associated with soil dust and resuspended road or construction dust, consistent with the active construct ion and road dust sources in the zone. The elevated Cl concentration was attributed to chlorine-containing raw materials and emissions from chemical and hazardous waste treatment facilities in the zone, as well as coal combustion. Overall, $PM_{2.5}$ mass was not strongly governed by inorganic element variability, as these elements constituted a relatively small and stable fraction of total $PM_{2.5}$.

Carbonaceous $PM_{2.5}$ was dominated by OC, with EC averaging 6.10 ± 3.95 μg/m$^3$. The mean OC/EC ratio was 1.86, indicating the influence of both primary combustion emissions and secondary organic aerosol formation. The temporal covariation in $PM_{2.5}$ and OC suggested that organic aerosols were a substantial contributor to $PM_{2.5}$ mass. Using the EC-tracer method with a conversion factor of 1.6, SOAs were estimated to account for 18.43% of $PM_{2.5}$ mass, indicating that secondary formation contributed significantly to the carbonaceous fraction of $PM_{2.5}$ in the CH High-Tech Zone.

### *3.2. Water-Soluble PM2.5 Ions*

#### 3.2.1. Characteristics and Source Identification

During the sampling period, water-soluble ion concentrations ranged from 17.14 to 92.43 μg/m$^3$, accounting for 23.3% to 92% of the $PM_{2.5}$ mass, as shown in Figure 2. The ion concentration order was as follows: $NO_3^-$ (16.43 ± 8.36 μg/m$^3$) > $Cl^-$ (8.81 ± 5.72 μg/m$^3$) > $SO_4^{2-}$ (8.41 ± 2.78 μg/m$^3$) > $NH_4^+$ (5.89 ± 3.53 μg/m$^3$) > $Na^+$ (4.52 ± 1.53 μg/m$^3$) > $K^+$ (0.91 ± 0.29 μg/m$^3$) > $Ca^{2+}$ (0.70 ± 0.60 μg/m$^3$) > $Mg^{2+}$ (0.058 ± 0.058 μg/m$^3$). The $NO_3^-$ /$SO_4^{2-}$ ratio is widely used as an indicator to distinguish the relative contributions of mobile and stationary sources to atmospheric $PM_{2.5}$. The persistently high $NO_3^-$ levels indicate that despite the significant success of $SO_2$ control measures in reducing sulfur dioxide emissions, nitrogen oxide emissions primarily stemming from industrial processes and motor vehicles remain at relatively high levels; this finding is consistent with the nitrate-dominated trend observed across China following the implementation of the Clean Air Action Plan [26].

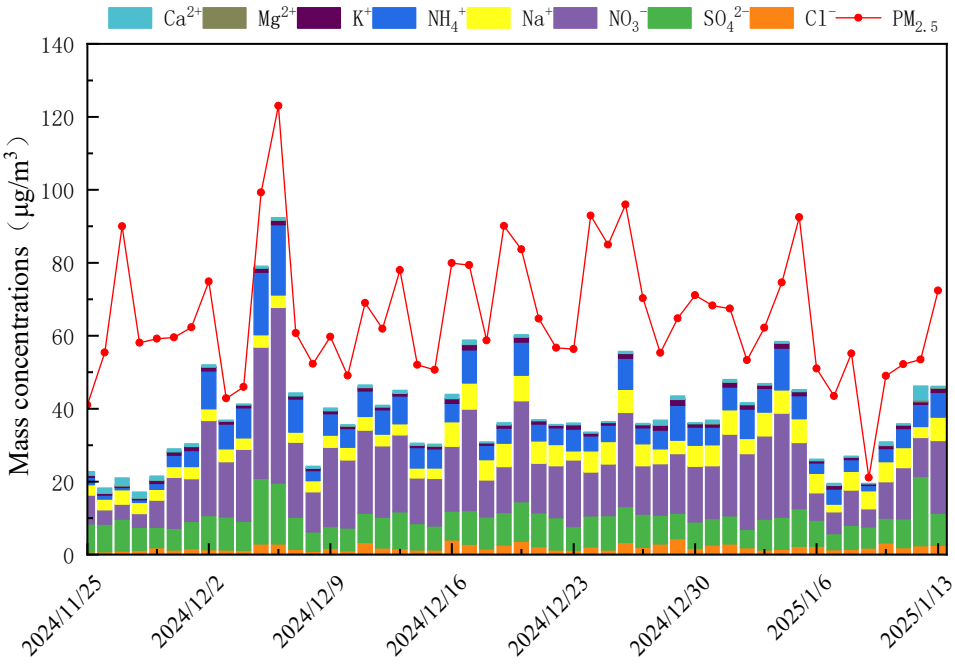



**Figure 2.** Temporal variation in $PM_{2.5}$ mass concentration and eight water-soluble ion species during the sampling campaign.

SIAs were the dominant components of the water-soluble ion fraction, with concentrations ranging from 10.80 to 84.10 μg/m$^3$ and accounting for 62.8–91% of total water-soluble ions. Spearman correlation analysis (shown in Figure S2) confirmed significant positive correlations between $PM_{2.5}$ and all major water-soluble ions, particularly $SO_4^{2-}$, $Na^+$, $NO_3^-$, $K^+$, $Cl^-$, and $NH_4^+$. The secondary ions were mutually correlated, with the strongest association being observed between $NH_4^+$ and $NO_3^-$, underscoring the critical role of ammonium nitrate formation in aerosol growth. $Mg^{2+}$ and $Ca^{2+}$ were also strongly correlated, suggesting common generation pathways, likely crustal/dust sources.

PCA of the eight water-soluble ions yielded three factors, as shown in Table 2 and Figure S3. Factor 1 was characterized by high loadings of $NO_3^-$ (0.892), $NH_4^+$ (0.870), $K^+$ (0.792), $Cl^-$ (0.718), and $SO_4^{2-}$ (0.557), representing a mixed source of secondary inorganic salts (from $SO_2$ and NOx oxidation) and cooking emissions ($K^+$ and $Cl^-$ from food ingredients and cooking processes). Factor 2 was dominated by $Mg^{2+}$ (0.957), $Ca^{2+}$ (0.948), and $SO_4^{2-}$ (0.640), indicative of a mixed dust and industrial source, where $Mg^{2+}$ and $Ca^{2+}$ are tracers of soil/construction dust and $SO_4^{2-}$ likely represents industrially emitted sulfate adsorbed onto dust particle surfaces. Factor 3 was loaded primarily with $Na^+$ (0.666) and $Cl^-$ (0.515), consistent with a cooking source attributable to dietary salt (NaCl) and potassium from food ingredients. These PCA results are consistent with the source categories subsequently resolved by the PMF model and provide independent evidence for the importance of secondary inorganic formation, industrial/dust emissions, and cooking as major sources of water-soluble ions in the CH High-Tech Zone.

**Table 2.** PCA of the water-soluble ions in CH High-Tech Zone.

| Ions | Factors | | |
|---|---|---|---|
| | PC1 | PC2 | PC3 |
| $NO_3^-$ | 0.892 | −0.066 | −0.368 |
| $NH_4^+$ | 0.870 | 0.052 | −0.466 |
| $K^+$ | 0.792 | −0.100 | 0.344 |
| $Cl^-$ | 0.718 | 0.171 | 0.515 |
| $Mg^{2+}$ | −0.112 | 0.957 | 0.133 |
| $Ca^{2+}$ | −0.189 | 0.948 | 0.169 |
| $SO_4^{2-}$ | 0.557 | 0.640 | −0.309 |
| $Na^+$ | 0.466 | −0.216 | 0.666 |
| Characteristic Value | 3.271 | 2.318 | 1.322 |
| Variance Contribution Rate (%) | 40.883 | 28.97 | 16.525 |
| Total Contribution Rate (%) | 40.883 | 69.854 | 86.378 |

#### 3.2.2. Secondary Transformation (SOR and NOR) and Acid–Base Balance of the Water-Soluble Ions

SOR and NOR can be used to characterize the extent of conversion of the gaseous precursors $SO_2$ and $NO_2$ into $SO_4^{2-}$ and $NO_3^-$, respectively. When both SOR and NOR were greater than 0.10, $SO_4^{2-}$ and $NO_3^-$ species in $PM_{2.5}$ primarily originate from the secondary transformation. Higher values of SOR and NOR indicate a greater extent of conversion of $SO_2$ and $NO_2$ gases into secondary-aerosol particles [27].

During the autumn and winter sampling period in the CH High-Tech Zone, SOR and NOR values are shown in Figure 3. The mean values of SOR and NOR were 0.365 ± 0.088 and 0.207 ± 0.077, respectively, indicating that $SO_4^{2-}$ and $NO_3^-$ in $PM_{2.5}$ were primarily formed through the secondary transformation of gaseous pollutants. Both ratios substantially exceed the 0.10 threshold, and the elevated SOR is particularly noteworthy, indicating efficient oxidation of $SO_2$ to sulfate despite declining ambient $SO_2$ concentrations.

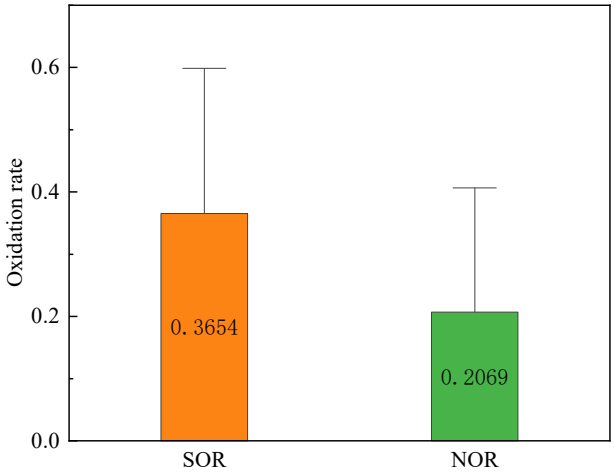



**Figure 3.** Distribution of SOR and NOR during the sampling campaign.

The acid–base balance of the water-soluble ions was evaluated from the anion and cation equivalent (AE and CE) concentrations:

$$AE = \frac{\rho(NO_3^-)}{62} + \frac{\rho(SO_4^{2-})}{48} + \frac{\rho(Cl^-)}{35.5} \quad (5)$$

$$CE = \frac{\rho(Na^+)}{23} + \frac{\rho(Mg^{2+})}{12} + \frac{\rho(K^+)}{39} + \frac{\rho(Ca^{2+})}{20} + \frac{\rho(NH_4^+)}{18} \quad (6)$$

The daily AE and CE values are strongly correlated ($R^2 = 0.9225$) with a regression slope of k = 1.0916; i.e., anion equivalents slightly exceed cation equivalents (in Figure S4). Using the campaign-mean concentrations, AE/CE = 1.17. The autumn–winter $PM_{2.5}$ in the CH High-Tech Zone is therefore neutral to slightly acidic, with a small excess of anions (mainly $NO_3^-$- and $Cl^-$) over the neutralizing cations (mainly $NH_4^+$).

### 3.2.3. Evolution Across Pollution Levels

To elucidate the drivers of $PM_{2.5}$ escalation, water-soluble ion concentrations were compared across four air quality levels defined by $PM_{2.5}$ concentrations: excellent (<35 μg/m$^3$), good (35–75 μg/m$^3$), light pollution (75–115 μg/m$^3$), and moderate pollution (115–150 μg/m$^3$). The numbers of daily samples in these classes are 18 days for the excellent level, 20 days for the good level, 11 days for light pollution and one day for moderate pollution (6 December 2024, 123 μg/m$^3$), because the highest class contains a single 24 h sample, comparisons involving the moderate level characterize that episode rather than a general concentration-dependent response, and a comparison merging the light and moderate classes gives the same conclusions. As shown in Figure 4, at the excellent level, total water-soluble ion concentration was relatively low at 19.56 μg/m$^3$. Transitioning to the good level, ion concentrations rose to 35.62 μg/m$^3$, driven primarily by an approximately 3-fold increase in $NH_4^+$, while $NO_3^-$ and $SO_4^{2-}$ each more than doubled. At the light-pollution level, all ions increased markedly, with $NO_3^-$ rising from 5 μg/m$^3$ (excellent) to 19.72 μg/m$^3$. The most dramatic increases occurred in the single moderate-pollution day (6 December 2024), where $NH_4^+$ and $NO_3^-$ surged approximately 12-fold and 9-fold, respectively, relative to excellent conditions, while $SO_4^{2-}$ increased approximately 3-fold. Given its high absolute concentration, $SO_4^{2-}$ retained a substantial mass contribution even at lower relative growth rates. That day was characterized by stagnant, humid conditions, which favor both accumulation and aqueous-phase ammonium nitrate formation; $NH_4^+$ and $NO_3^-$ were the highest of the campaign, with secondary ions accounting for 68.4% of $PM_{2.5}$.

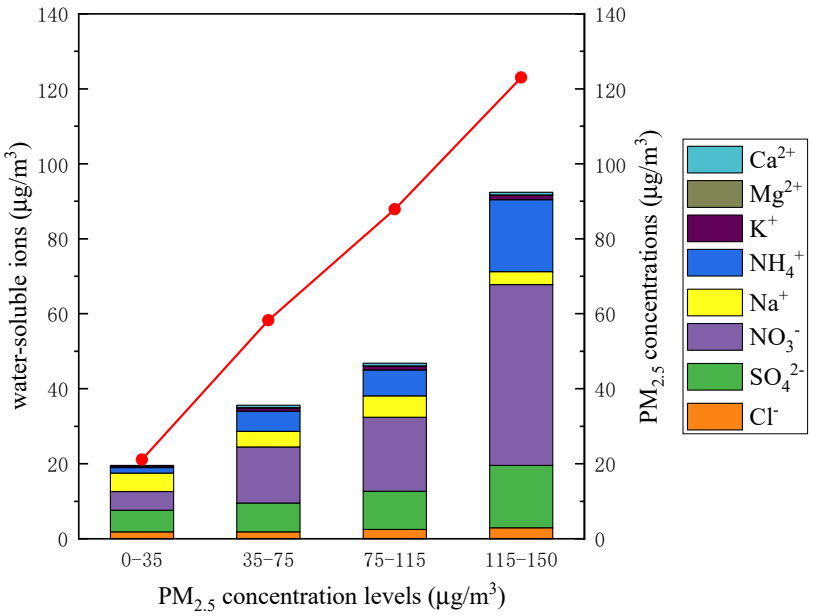



**Figure 4.** Variation in water−soluble ion concentration levels under different $PM_{2.5}$ concentration levels (18, 20 and 11 days for the excellent, good, and light−pollution levels; the moderate class comprises a single day, 6 December 2024).

These findings demonstrate that the concurrent rise in $NH_4^+$, $NO_3^-$, and $SO_4^{2-}$, particularly $NH_4^+$ and $NO_3^-$, marks secondary-aerosol formation as the dominant contributor to $PM_{2.5}$ mass increases during autumn–winter pollution episodes. These ionic species are not emitted directly and do not themselves drive emissions; rather, shared gaseous precursors (NOx, $SO_2$ and $NH_3$) and common combustion, and industry-related sources elevate the primary dust fraction and the secondary ion fraction simultaneously. The disproportionate growth of ammonium nitrate suggests that reductions in NOx and $NH_3$ emissions would yield the greatest marginal benefits for $PM_{2.5}$ mitigation in this region, aligning with recent studies emphasizing the critical role of nitrate in wintertime haze formation and the need for coordinated NOx–$NH_3$ control strategies.

### *3.3. Source Apportionment Using the PMF Method*

#### 3.3.1. Direct PMF Source Apportionment

The EPA PMF 5.0 model was employed for source apportionment, with 25 chemical species as input data. A total of seven major source factors were identified, as shown in Figure 5.

Factor 1, Coal Combustion: Characterized by the highest $Cl^-$ loading, accompanied by EC, Al, and $Ca^{2+}$, as well as moderate levels of $SO_4^{2-}$ and POC. $Cl^-$, EC, Al, and $Ca^{2+}$ are well-established tracers of coal combustion, while $SO_4^{2-}$ reflects the secondary oxidation of $SO_2$ resulting from coal combustion [28]. This factor is consistent with the presence of large coal-fired power plants and other industrial coal-fired boilers within the monitoring area. Factor 2, Mobile Source: Primarily comprising EC and POC. EC serves as a marker for incomplete fossil fuel combustion (particularly in diesel vehicle exhaust), while POC may either originate alongside EC from diesel exhaust or be associated with biomass combustion [29,30]. This factor reflects motor vehicle emissions from the dense road network and highways surrounding the monitoring station. Factor 3, Food Service: Characterized by POC, $Na^+$, and $Cl^-$. The decomposition of high-temperature cooking oils generates organic aerosols rich in POC; $Na^+$ and $Cl^-$ originate from table salt (NaCl), while $K^+$ comes from the ingredients or from the combustion of the cooking stove.

The monitoring station is located on the school campus, surrounded by residential areas and restaurants, which is consistent with the significant contribution of the food service source. Factor 4, Secondary Inorganic Salts: Loaded with $NH_4^+$, $NO_3^-$, $SO_4^{2-}$, and S. These species are products of the gas–particle transformation of $SO_2$, NOx, and $NH_3$, originating respectively from coal combustion, motor vehicle exhausts and industrial processes. The strong correlation between sulfate and ammonium ions indicates that ammonium sulfate is an important species, likely associated with coal-fired power plants. Factor 5, Other Sources: A mixed category without a dominant tracer source, representing unresolved sources or multiple minor contributions. Factor 6, Dust Source: Enriched in Al, Si, Ba, Ca, and Fe. Al and Si are primary components of soil and serve as indicators of the re-suspension of soil dust, construction dust, or road dust. Ca and Ba are indicators of construction materials. This factor encompasses soil dust, construction dust, and road dust, collectively referred to as dust sources. Factor 7, Industrial Source: Characterized by Zn, Cl, and Fe. Zn and Fe are associated with industrial activities such as casting and machining; Cl originates from chemical processing and hazardous waste treatment processes. Analysis of dust samples collected from local casting and iron-smelting enterprises confirmed high Zn content, thereby validating the attribution of this source [31]. Given that simultaneously incorporating POC and EC as independent species would introduce identical temporal signals into the matrix, potentially altering their effective weights relative to other species, we added a set of sensitivity analyses that excluded POC input, and the results show that relative contributions of the seven source categories are materially unchanged between the two runs (Figure S5).

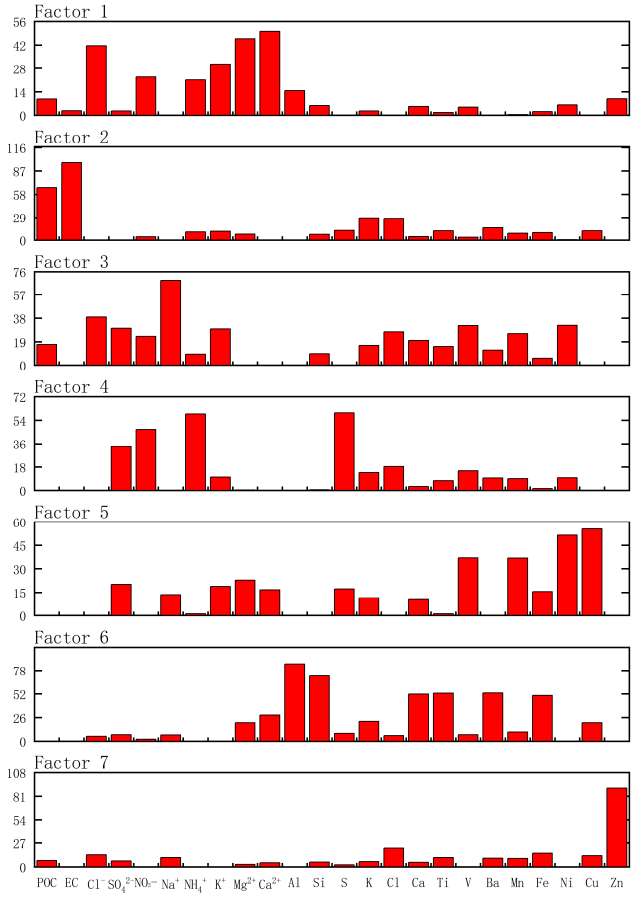



**Figure 5.** Direct PMF source apportionment results for the overall $PM_{2.5}$ sources during the autumn and winter seasons in the CH High-Tech Zone.

3.3.2. Inventory-Constrained Reapportionment of the Secondary Fraction

During autumn and winter, the pre-estimated SOAs accounted for 18.43% of $PM_{2.5}$ mass and the fraction other than the pre-estimated SOAs. The directly PMF-resolved source contributions are industrial source (13.42%) > dust source (11.9%) > catering source (11.69%) > coal combustion source (11.4%) > secondary inorganic salts (11.39%) > mobile source (11.15%) > other source categories (10.62%), in addition to the pre-estimated SOAs (18.43%).

In the subsequent assumption-dependent step (Section 2.3.2), the PMF-resolved SIAs and the pre-estimated SOAs were distributed to primary source categories according to the sectoral $SO_2$ + NOx and VOC emission shares in the atmospheric emission source inventory. The reapportioned results presented in Figure 6 are: industrial source (39.58%) > mobile source (14.64%) > dust source (11.9%) > catering source (11.86%) > coal combustion source (11.4%) > other source categories (10.62%). The allocation keys and the full calculation are documented in Table S1.

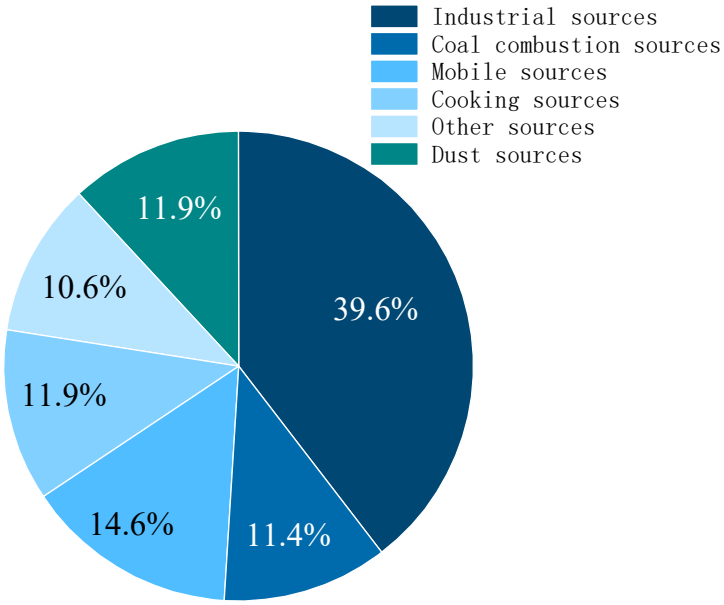



**Figure 6.** Source apportionment results for $PM_{2.5}$ in the CH High-Tech Industrial Development Zone during autumn and winter seasons.

The industrial source represents the largest contributor, reflecting the high density of industrial enterprises within the CH High-Tech Industrial Development Zone. Industrial activities emit large quantities of primary particulate matter, as well as significant amounts of secondary precursors, such as NOx, $SO_2$, and $VOC_S$. These industrial emissions not only drive the direct particulate matter load but also contribute to the formation of the majority of secondary inorganic and organic aerosols. The presence of chemical plants and hazardous waste treatment facilities further contributes to the formation of chlorine-containing species. The mobile source represents the second-largest contributor. Motor vehicles emit NOx, $VOC_S$, black carbon, CO, and flue gas; among these, NOx and $VOC_S$ serve as key precursors for the formation of nitrates and SOAs. The growth in the regional motor vehicle fleet, combined with upstream and downstream mobile-related emissions as well as the resuspension of road dust, has amplified the overall impact of mobile source.

In summary, the comprehensive source apportionment analysis indicates that $PM_{2.5}$ concentrations during the autumn and winter seasons in the CH High-Tech Zone are predominantly driven by industrial emissions, followed by mobile source, fugitive dust, catering activities, and coal combustion. Secondary aerosols account for a significant

proportion of the total $PM_{2.5}$, primarily attributable to precursor emissions from industrial and mobile sources; this underscores the need for a dual-control strategy that simultaneously targets both primary particulate matter emissions and gaseous precursors (NOx, $SO_2$, $VOC_S$, and $NH_3$). The prominent role of ammonium nitrate in driving the worsening of air pollution further demonstrates that the coordinated control of NOx and $NH_3$ emissions is crucial to effectively mitigating $PM_{2.5}$ levels in this industrial area.

## 4. Discussion

This study conducted a systematic chemical characterization and source apportionment analysis of $PM_{2.5}$ in the CH High-Tech Zone, in the western Yangtze River Delta, based on 50 daily $PM_{2.5}$ samples collected between November 2024 and January 2025. Water-soluble ions, carbonaceous components and inorganic elements were characterized, and source apportionment was performed with the EPA PMF 5.0 model, supported by PCA and SOA estimation. The key conclusions are as follows.

During the sampling period, $PM_{2.5}$ pollution was associated with low wind speeds, high RH, and northerly winds transporting industrial emissions. Water-soluble ions dominate the chemical composition of $PM_{2.5}$, followed by carbonaceous components and inorganic elements. Among the water-soluble ions, $NO_3^-$, $SO_4^{2-}$, and $NH_4^+$ are the dominant ionic species, and the $NO_3^-/SO_4^{2-}$ ratio indicates the growing importance of mobile and industrial NOx emissions relative to stationary SO2 sources. SOR and NOR confirm the significant secondary transformation of gaseous precursors. PCA of water-soluble ions identified three primary source categories: secondary inorganic salt–food service mixtures, dust–industrial mixtures, and food service sources. Analysis of different pollution levels revealed that from excellent to moderate-pollution levels, the concentrations of $NH_4^+$ and $NO_3^-$ increased approximately 12-fold and 9-fold, respectively, indicating that ammonium nitrate is the key driving factor behind the intensification of $PM_{2.5}$ pollution during autumn and winter; these fold changes characterize the single moderate-pollution day (6 December 2024) and are corroborated by the 11-day light-pollution class. PMF resolved seven source categories; after reapportioning the secondary fraction to primary emission categories based on the local emission inventory, the industrial source was the largest contributor (39.6%), followed by mobile source and fugitive dust. Several limitations should be noted. First, the reapportionment of SIAs and SOAs is a first-order source attribution based on precursor-emission shares and does not account for the non-linear $NH_3$-NOx-$SO_2$ chemistry, atmospheric oxidation capacity or aerosol liquid water. Second, sector-resolved $NH_3$ emissions are not available in the emission inventory used, so the SIA allocation is presented as a first-order estimate based on precursor-emission shares.

The findings indicate that effective $PM_{2.5}$ mitigation in the CH High-Tech Zone during autumn and winter should prioritize the control of industrial emissions, and given the dominant role of ammonium nitrate in driving the escalation of pollution levels, the coordinated reduction in NOx and $NH_3$ emissions is particularly critical. Supporting measures should target mobile source emissions, dust control, management of catering cooking fumes, and the transition to clean energy alternatives for coal-fired facilities.

**Supplementary Materials:** The following supporting information can be downloaded at: https://www.mdpi.com/article/10.3390/atmos17111144/s1. Table S1. Inventory-based reapportionment keys and calculation. Table S2. Carbon fractions by the EC-tracer method. Figure S1. Time series of AQI, $PM_{2.5}$, $SO_2$, $NO_2$, temperature, humidity, and wind vector at automatic monitoring stations during the sampling period. Figure S2. Correlation between $PM_{2.5}$ and water-soluble ions during the sampling period. Figure S3. The PCA of the water-soluble ions in CH High-Tech Zone. Figure S4. Cation–anion equivalent balance of the water-soluble ions. Figure S5. Direct PMF source apportionment results for

the overall $PM_{2.5}$ sources (without POC) during the autumn and winter seasons in the CH High-Tech Zone. Text S1. Chemical analysis processes. Text S2. Meteorological conditions.

**Author Contributions:** Conceptualization, X.H. and L.J.; Data curation, X.H. and C.Y.; Formal analysis, X.H. and C.Y.; Funding acquisition, L.J. and X.Z.; Methodology, X.H. and C.Y.; Project administration, X.Z.; Software, X.H. and C.Y.; Validation, Y.L. and L.Z.; Writing—original draft, X.H.; Writing—review and editing, L.J., J.F. and X.Z. All authors have read and agreed to the published version of the manuscript.

**Funding:** This research was funded by the Central Public interest Scientific Institution Basal Research Fund, China (GYZX250106; GYZX20260316).

**Institutional Review Board Statement:** Not applicable.

**Informed Consent Statement:** Not applicable.

**Data Availability Statement:** Data will be made available upon request.

**Conflicts of Interest:** The authors declare no conflicts of interest.

## References

1. Du, W.; Zhang, Y.; Chen, Y.; Xu, L.; Chen, J.; Deng, J.; Hong, Y.; Xiao, H. Chemical Characterization and Source Apportionment of PM2.5 during Spring and Winter in the Yangtze River Delta, China. *Aerosol Air Qual. Res.* **2017**, *17*, 2165–2180. [CrossRef]
2. Zhang, Y.; Tian, J.; Wang, Q.; Qi, L.; Manousakas, M.I.; Han, Y.; Ran, W.; Sun, Y.; Liu, H.; Zhang, R.; et al. High-Time-Resolution Chemical Composition and Source Apportionment of PM 2.5 in Northern Chinese Cities: Implications for Policy. *Atmos. Chem. Phys.* **2023**, *23*, 9455–9475. [CrossRef]
3. Huang, R.-J.; Zhang, Y.; Bozzetti, C.; Ho, K.-F.; Cao, J.-J.; Han, Y.; Daellenbach, K.R.; Slowik, J.G.; Platt, S.M.; Canonaco, F.; et al. High Secondary Aerosol Contribution to Particulate Pollution during Haze Events in China. *Nature* **2014**, *514*, 218–222. [CrossRef] [PubMed]
4. Cao, J.-J.; Shen, Z.-X.; Chow, J.C.; Watson, J.G.; Lee, S.-C.; Tie, X.-X.; Ho, K.-F.; Wang, G.-H.; Han, Y.-M. Winter and Summer $PM_{2.5}$ Chemical Compositions in Fourteen Chinese Cities. *J. Air Waste Manag. Assoc.* **2012**, *62*, 1214–1226. [CrossRef] [PubMed]
5. Sun, X.; Zhao, T.; Hu, J.; Bai, Y.; Meng, L.; Yang, Q.; Zhou, Y.; Fu, W. Inverse Effects of Aerosol Radiative Forcing on Heavy PM 2.5 Pollution of Local Accumulation and Regional Transport over Central China. *Sci. Total Environ.* **2024**, *917*, 170319. [CrossRef] [PubMed]
6. Zhang, Q.; Zheng, Y.; Tong, D.; Shao, M.; Wang, S.; Zhang, Y.; Xu, X.; Wang, J.; He, H.; Liu, W.; et al. Drivers of Improved $PM_{2.5}$ Air Quality in China from 2013 to 2017. *Proc. Natl. Acad. Sci. USA* **2019**, *116*, 24463–24469. [CrossRef] [PubMed]
7. Turpin, B.J.; Lim, H.-J. Species Contributions to PM2.5 Mass Concentrations: Revisiting Common Assumptions for Estimating Organic Mass. *Aerosol Sci. Technol.* **2001**, *35*, 602–610. [CrossRef]
8. Guan, H.; Chen, Z.; Tian, J.; Xiao, H. Assessing PM2.5 Dynamics and Source Contributions in Southwestern China: Insights from Winter Haze Analysis. *Atmosphere* **2024**, *15*, 855. [CrossRef]
9. Zhang, Y.-L.; Cao, F. Fine Particulate Matter (PM2.5) in China at a City Level. *Sci. Rep.* **2015**, *5*, 14884. [CrossRef] [PubMed]
10. Diao, Y.; Liu, A.; Hu, Q.; Yang, M.; Zhao, T.; Cui, Y.; Shi, S.; Kong, X. Characteristics of Chemical Composition and Source Apportionment of PM2.5 during a Regional Haze Episode in the Yangtze River Delta, China. *Front. Environ. Sci.* **2022**, *10*, 1027397. [CrossRef]
11. Xu, J.; Zhang, Y.; Wang, Y.; Yan, X.; Zhu, B.; Lu, C.; Yang, Y.; Sun, Y.; Zhang, J.; Zuo, X.; et al. Measurement Report: Insights into Seasonal Dynamics and Planetary Boundary Layer Influences on Aerosol Chemical Components in Suburban Nanjing from One-Year Observation. *Atmos. Chem. Phys.* **2025**, *25*, 18599–18616. [CrossRef]
12. Wang, Q.; Deng, W.; Tu, X.; Wang, J.; He, D.; Gong, Y.; Tan, Z.; Lu, K. Spatial Variations in PM2.5 Composition and Source Apportionment across Six Cities of Jiangxi, China: Insights from the 2023–2024 New Year Haze Episode. *Front. Environ. Sci.* **2025**, *13*, 1622013. [CrossRef]
13. Liu, Z.; Qi, J.; Ni, Y.; Xue, L.; Liu, X. Enhanced Atmospheric Oxidation and Particle Reductions Driving Changes to Nitrate Formation Mechanisms across Coastal and Inland Regions of North China. *Atmos. Chem. Phys.* **2025**, *25*, 8719–8742. [CrossRef]
14. Tang, K.; Zhang, H.; Xu, G.; Chang, F.; Xu, Y.; Miao, J.; Cui, X.; Jin, J.; Li, B.; Li, K.; et al. Optimizing Ammonia Emissions for $PM_{2.5}$ Mitigation: Environmental and Health Co-Benefits in Eastern China. *Atmos. Chem. Phys.* **2025**, *25*, 14747–14762. [CrossRef]
15. Zang, H.; Zhao, Y.; Huo, J.; Zhao, Q.; Fu, Q.; Duan, Y.; Shao, J.; Huang, C.; An, J.; Xue, L.; et al. High Atmospheric Oxidation Capacity Drives Wintertime Nitrate Pollution in the Eastern Yangtze River Delta of China. *Atmos. Chem. Phys.* **2022**, *22*, 4355–4374. [CrossRef]

16. Wang, Y.; Yao, L.; Wang, L.; Liu, Z.; Ji, D.; Tang, G.; Zhang, J.; Sun, Y.; Hu, B.; Xin, J. Mechanism for the Formation of the January 2013 Heavy Haze Pollution Episode over Central and Eastern China. *Sci. China Earth Sci.* **2014**, *57*, 14–25. [CrossRef]
17. Paatero, P.; Tapper, U. Positive Matrix Factorization: A Non-Negative Factor Model with Optimal Utilization of Error Estimates of Data Values. *Environmetrics* **1994**, *5*, 111–126. [CrossRef]
18. Song, Y.; Zhang, Y.; Xie, S.; Zeng, L.; Zheng, M.; Salmon, L.G.; Shao, M.; Slanina, S. Source Apportionment of PM2.5 in Beijing by Positive Matrix Factorization. *Atmos. Environ.* **2006**, *40*, 1526–1537. [CrossRef]
19. Zhang, R.; Jing, J.; Tao, J.; Hsu, S.-C.; Wang, G.; Cao, J.; Lee, C.S.L.; Zhu, L.; Chen, Z.; Zhao, Y.; et al. Chemical Characterization and Source Apportionment of $PM_{2.5}$ in Beijing: Seasonal Perspective. *Atmos. Chem. Phys.* **2013**, *13*, 7053–7074. [CrossRef]
20. Behera, S.N.; Sharma, M. Investigating the Potential Role of Ammonia in Ion Chemistry of Fine Particulate Matter Formation for an Urban Environment. *Sci. Total Environ.* **2010**, *408*, 3569–3575. [CrossRef] [PubMed]
21. Guo, L.; Gu, C.; Dong, K.; Ou, S.; Zhao, X.; Wang, X.; Zheng, Z.; Yang, W. Composition Characteristics and Potential Regions of PM2.5 during Winter Haze Pollution in Typical Industrial Areas, NW-China. *Aerosol Air Qual. Res.* **2024**, *24*, 230290. [CrossRef]
22. Cui, Q.; Sun, J.; Fan, Y.; Li, Y. Characterisation and Source Apportionment of Chemical Components in Fine Particulate Matter from Atmosphere in Two Districts of Lanzhou City. *Environ. Chem.* **2024**, *21*, EN24057. [CrossRef]
23. Wang, S.; Wang, Q.; Zhang, T.; Liu, S.; Ho, S.S.H.; Tian, J.; Su, H.; Zhang, Y.; Wang, L.; Wu, T.; et al. Elaborations of the Influencing Factors on the Formation of Secondary Inorganic Aerosols in a Heavily Polluted Urban Area of China. *J. Environ. Sci.* **2024**, *138*, 406–417. [CrossRef] [PubMed]
24. Jeon, J.-W.; Park, S.-W.; Han, Y.-J.; Lee, T.; Lee, S.-H.; Park, J.-M.; Yoo, M.-S.; Shin, H.-J.; Hopke, P.K. Nitrate Formation Mechanisms Causing High Concentration of PM2.5 in a Residential City with Low Anthropogenic Emissions during Cold Season. *Environ. Pollut.* **2024**, *352*, 124141. [CrossRef] [PubMed]
25. Jeong, M.J.; Hwang, S.-O.; Yoo, H.-J.; Oh, S.M.; Jang, J.; Lee, Y.; Kim, T.; Kim, S. Chemical Composition and Source Apportionment of PM2.5 in Seoul during 2018–2020. *Atmos. Pollut. Res.* **2024**, *15*, 102077. [CrossRef]
26. Tu, X.; Fang, X.; Fang, H.; Ye, C.; Liu, Z.; Jia, X.; He, D.; Wang, J.; Huang, H.; Zou, C.; et al. Chemical Composition Characteristics and Source Apportionment of PM2.5 in Ceramic Industrial Base during Winter. *Aerosol Air Qual. Res.* **2022**, *22*, 210390. [CrossRef]
27. Huang, X.; Liu, Z.; Zhang, J.; Wen, T.; Ji, D.; Wang, Y. Seasonal Variation and Secondary Formation of Size-Segregated Aerosol Water-Soluble Inorganic Ions during Pollution Episodes in Beijing. *Atmos. Res.* **2016**, *168*, 70–79. [CrossRef]
28. Zou, Y.; Liu, X.; Wu, K.; Zhou, Z.; Xu, M. The Effect of Multiple Factors on Changes in Organic-Inorganic Fractions of Condensable Particulate Matter during Coal Combustion. *Chemosphere* **2024**, *353*, 141638. [CrossRef] [PubMed]
29. Cui, M.; Chen, Y.; Tian, C.; Zhang, F.; Yan, C.; Zheng, M. Chemical Composition of PM 2.5 from Two Tunnels with Different Vehicular Fleet Characteristics. *Sci. Total Environ.* **2016**, *550*, 123–132. [CrossRef] [PubMed]
30. Martin, J.W.; Salamanca, M.; Kraft, M. Soot Inception: Carbonaceous Nanoparticle Formation in Flames. *Prog. Energy Combust. Sci.* **2022**, *88*, 100956. [CrossRef]
31. Xu, Y.; Zhang, W.; Huo, T.; Streets, D.G.; Wang, C. Investigating the Spatio-Temporal Influences of Urbanization and Other Socioeconomic Factors on City-Level Industrial NOx Emissions: A Case Study in China. *Environ. Impact Assess. Rev.* **2023**, *99*, 106998. [CrossRef]

**Disclaimer/Publisher's Note:** The statements, opinions and data contained in all publications are solely those of the individual author(s) and contributor(s) and not of MDPI and/or the editor(s). MDPI and/or the editor(s) disclaim responsibility for any injury to people or property resulting from any ideas, methods, instructions or products referred to in the content.